Atmospheric
Measurement
Techniques
Open Access
Discussions

The Backscatter Cloud Probe – a compact low-profile autonomous optical spectrometer

K. Beswick[1], D. Baumgardner[2], M. Gallagher[1], and R. Newton[2]

[1]University of Manchester, Manchester, UK
[2]Droplet Measurement Technologies, Boulder, CO, USA

Correspondence to: D. Baumgardner (darrel.baumgardner@gmail.com) and
K. Beswick (karl.beswick@manchester.ac.uk)

Discussion Paper | Discussion Paper | Discussion Paper | Discussion Paper |

AMTD
6, 7379–7424, 2013

The Backscatter Cloud Probe

K. Beswick et al.

Title Page

Abstract | Introduction

Conclusions | References

Tables | Figures

|◀ | ▶|

◀ | ▶

Back | Close

Full Screen / Esc

Printer-friendly Version

Interactive Discussion

The Backscatter Cloud Probe

K. Beswick et al.

Abstract

A compact (500 cm^3), lightweight (500 g), near-field, single particle backscattering optical spectrometer is described that mounts flush with the skin of an aircraft and measures the concentration and optical equivalent diameter of particles from 5 to 75 µm. The Backscatter Cloud Probe (BCP) was designed as a real-time qualitative cloud detector primarily for data quality control of trace gas instruments developed for the climate monitoring instrument packages that are being installed on commercial passenger aircraft as part of the European Union In-Service Aircraft for a Global Observing System (IAGOS) program (http://www.iagos.org/). Subsequent evaluations of the BCP measurements on a number of research aircraft, however, have revealed it capable of delivering quantitative particle data products including size distributions, liquid water content and other information on cloud properties. We demonstrate the instrument's capability for delivering useful long-term climatological information, across a wide range of environmental conditions.

The BCP has been evaluated by comparing its measurements with those from other cloud particle spectrometers on research aircraft and several BCPs are currently flying on commercial A340/A330 Airbus passenger airliners. The design and calibration of the BCP is described in this presentation, along with an evaluation of measurements made on the research and commercial aircraft. Comparisons of the BCP with two other cloud spectrometers, the Cloud Droplet Probe (CDP) and the Cloud and Aerosol Spectrometer (CAS), show that the BCP size distributions agree well with those from the other two, given the intrinsic limitations and uncertainties related to the three instruments. Preliminary results from more than 7000 h of airborne measurements by the BCP on two Airbus A-340s operating on routine global traffic routes (one Lufthansa, the other China Airlines) show that more than 340 h of cloud data have been recorded at normal cruise altitudes (> 10 km) and more than 40 % of the > 1200 flights were through clouds at some point between takeoff and landing. These data are a valuable contribution to data bases of cloud properties, including sub-visible cirrus, in the upper troposphere

and useful for validating satellite retrievals of cloud water and effective radius as well as providing a broader, geographically and climatologically relevant view of cloud microphysical variability useful for improving parameterizations of clouds in climate models. They are also useful for monitoring the vertical climatology of clouds over airports, especially those over mega-cities where pollution emissions may be impacting local and regional climate.

1 Background

Reliable predictions of the future climate using ever improving climate models are fundamental requirements for determining future mitigation strategies. The need for 3-D global data sets is increasing, particularly in those regions of the atmosphere where satellites are technically limited. Use of commercial aircraft now allows the collection and transmission of highly relevant observations on a scale and in numbers impossible to achieve using normal research aircraft. The European Research Infrastructure program IAGOS (In-service Aircraft for a Global Observing System) has therefore been developed with the aim of establishing a distributed infrastructure comprising a fleet of 10–20 long-range, in-service aircraft of internationally operating airlines for long-term observations of atmospheric composition on global scales to address the growing need of the global modeling community. The project, led by the Max Planck Institute of Biogeochemistry in collaboration with Airbus and commercial carriers, has developed several miniature modular instrument packages for commercial Airbus A330/A340 passenger aircraft. These expandable platforms currently include measurements of aerosol particle concentrations, reactive and greenhouse gases and, the focus of this presentation, cloud particle concentrations. Whilst the scientific community has learned a great deal about cloud microphysical processes and cloud radiative effects over the last few decades, most of the current global cloud data sets are either in situ measurements from short term field experiments or remote sensing data products, e.g. ISCCP, (International Cloud Satellite Cloud Climatology Project) established in 1982

The Backscatter Cloud Probe

K. Beswick et al.

Title Page

Abstract | Introduction

Conclusions | References

Tables | Figures

◄ | ►

◄ | ►

Back | Close

Full Screen / Esc

Printer-friendly Version

Interactive Discussion

as part of the World Climate Research Program. Currently the data products available to the community include cloud amount, cloud type and cloud top temperature as well as optical thickness based on radiance. More specific retrieved microphysical properties include effective liquid water and ice crystal particle radius which have been validated against a wide range of WCRP and GEWEX field campaigns e.g. GEWEX Cloud System Study Data Integration for Model Evaluation (GCCS-DIME) program. Typical uses for such global cloud data products are described by Rossow et al. (2005) who use cluster analysis techniques to investigate links between multi-variate relationships between clouds, mesoscale meteorological processes and global and regional energy-water budgets. Such studies are normally constrained to large fields of view and the inherent variability on sub-satellite, sub-grid scales are lost. Field campaigns to study these sub-grid scale processes, however, are expensive and time consuming to mount and are often time limited. In this respect a continuous, real-time, in situ observing system can make a contribution by providing key data products.

The remainder of this presentation introduces a new instrument, the Backscatter Cloud Probe (BCP) whose design was originally for a simple instrument that would detect the presence of cloud. The design and operating principles are described, analysis techniques detailed and flight tests and measurements from commercial airliners discussed.

2 Backscatter Cloud Probe

2.1 Design and operating principals

The BCP optical layout, as shown in Fig. 1a, consists of a laser diode that produces focused, linearly polarized light at a wavelength of 680 nm. The beam is focused to a small region approximately 4 cm from the fused, silicate glass window through which the laser is transmitted. Particles that pass through this region of the beam scatter light with an intensity that depends upon the size and shape of the particle and the angle

with respect to the incident beam. The fraction of light that is scattered backward at a solid angle of 144°–156° is collected by a set of lenses that are located behind the window and that focus the collected light onto an avalanche photodiode (APD). The sensitive sample area of the beam, as well as the collection angles, is determined by the width of the laser beam at the center of focus of the optics and the diameter of the lens. As will be discussed in the following sections, the close proximity of the sample area to the fuselage, and the shape of the sample area have to be taken into account when processing the measurements and estimating uncertainties.

The photons that strike the APD are converted into a current that is subsequently transmitted to signal conditioning electronics that change the current to a voltage, filter out electronic noise and remove offsets that may arise due to the capacitive elements in the electronic circuit. The peak of the transient signal formed as an individual particle passes through the laser is detected and digitized by a 4096 bit analog to digital converter. The value of this peak is used to select one of 10 channels to increment by one count (in the current version of the BCP used on the commercial aircraft). The thresholds of these 10 channels are set based upon calibrations and theory as further detailed below. In addition to creating the 10 channel histogram of counts, various voltages and temperatures, "housekeeping" parameters are measured for monitoring the health of the instrument. The size histogram and housekeeping parameters are transmitted serially when given a command by a data system.

The compact, simple design of the BCP optical head, which weighs only 500 g and takes up a volume of less than 500 cm^3, allows it to be mounted easily. Thousands of hours of flying on commercial aircraft (discussed in Sect. 3.2) show that it requires infrequent maintenance. Figure 1b shows the physical form of the BCP and Fig. 2 shows the BCP compared to two other single particle optical spectrometers, the cloud droplet probe (CDP), which was introduced in 2003, and the forward scattering spectrometer probe (FSSP), developed in 1976, illustrating how state of the art optics and electronics has allowed the scaling down in size and weight of cloud spectrometers. One of the disadvantages of the BCP is that the laser currently used is not eye-safe and so

The Backscatter Cloud Probe

K. Beswick et al.

Title Page

Abstract | Introduction

Conclusions | References

Tables | Figures

◄◄ | ►►

◄ | ►

Back | Close

Full Screen / Esc

Printer-friendly Version

Interactive Discussion

precautions are needed so as not to operate it under conditions where it could be a potential hazard. The next generation BCP, under development, will use an eye-safe laser.

The BCP is designed to mount on the interior of an aircraft looking out through a transparent aperture. Figure 3 shows photos of three installations of a BCP: (a) mounted on the hatch of the Facility for Airborne Atmospheric Measurements (FAAM) BAE-146, (b) on the nose of the University of North Dakota Cessna Citation and (c) on the nose of the Lufthansa "Veirsen" A340-300 Airbus.

The BCP was designed to meet the specifications of the In-Service Aircraft for a Global Observing System (IAGOS) program. The principal use of the BCP was intended as a simple indicator of the presence of cloud for input in analyzing the other measurements that are part of the IAGOS package, i.e. water vapor, ozone, carbon monoxide, etc. The BCP was designed, however, to function under the same principles as other single particle cloud spectrometers, i.e. to estimate particle sizes based upon the intensity of light scattered by the particle as it passes through the laser beam. Hence, it not only detects the presence of a cloud but also provides additional information about its microphysical properties via distributions of number and mass concentrations derived under certain necessary assumptions discussed below.

As will also be further elaborated in the following sections, there are potential limitations that are related to the distance from the aircraft skin to the sensitive sample volume and also to the non-uniform laser intensity within this sample volume. The first issue is discussed in Sect. 3 while the second issue is the subject of the following two sections.

2.2 Calibration

The intensity distribution across the diode laser beam is approximately Gaussian such that when a particle passes through the laser beam, within the viewing volume that is defined by the collection optics, it has the probability of passing through different laser

Title Page

Abstract | Introduction

Conclusions | References

Tables | Figures

◄◄ | ►►

◄ | ►

Back | Close

Full Screen / Esc

Printer-friendly Version

Interactive Discussion

intensities, i.e. particles with the same optical diameter can scatter different amounts of light due to the variation in beam intensity across its cross section.

In a cloud with a range of particle sizes, the measured size distribution will represent the sum of the probability distributions of each particle size category determined by the probabilities that a particle will pass through a specific intensity region of the beam. Given that we have an accurate measurement of the intensity distribution of the laser beam across the sensitive beam area, we are faced with the classic inversion problem of estimating the ambient size distribution from the measured distribution. The implementation of this inversion is described in the following Sect. 2.3.

The intensity distribution of the sample area is measured using a beam mapper, similar to the one described by Lance et al. (2010), in which a linear, mono-dispersed droplet stream is produced by a piezoelectric oscillator that breaks up a narrow stream of water into droplets that are directed through the laser beam of the BCP by a micro-positioner with an accuracy of 10 μm. The maximum scattering intensity registered by the BCP is monitored and by rastering along and across the laser beam, an intensity map is created, such as the one shown in Fig. 4. The colors represent the relative intensity of scattering from the particles, where red is maximum and blue is minimum. The mapping of the beam also provides a measure of the sensitive sample area of the BCP which, in this case, was determined to be $0.18 \pm 0.014\,\text{mm}^2$. In this example, 22 μm droplets were used to map the area.

The droplet diameter is derived from the "glare" (Korolev et al., 1991; Wendisch et al., 1996; Nagel et al., 2007), in which specular reflections off the front and back face of droplets are observed by a camera. These droplets of known diameter are used to map the laser beam, and since their scattering cross sections can be calculated directly with Mie theory (Mie, 1908), they are used to calibrate the BCP for size. The scattering cross section provides the relationship between the voltage, V_0, produced by the photodetector and its associated electronics, and the scattered light intensity, I_0. The scale factor $S = I_0/V_0$ is used to calculate scattering cross sections from the measured peak voltages. The value of V_0 is obtained when the calibration water droplet passes through

Title Page

Abstract | Introduction

Conclusions | References

Tables | Figures

|◄ | ►|

◄ | ►

Back | Close

Full Screen / Esc

Printer-friendly Version

Interactive Discussion

the maximum beam intensity. All of the calculations described in Sect. 2.3 are scaled according to this value.

As an idealized example, if the laser intensity within the sensitive sample area is uniform and homogeneous in intensity, then to derive the optical diameter of a cloud droplet, all that is needed is the measured voltage, V, multiplied by S to obtain a scattering cross section, I, that is associated with a diameter of droplet, D; however, due to the non-uniform intensity of the laser beam, as well as the non-monotonic relationship between particles and their scattering cross section in the Mie scattering region, a more complex procedure is needed to retrieve the particle sizes as described below.

2.3 Data retrieval

The derivation of size distributions from the ambient backscatter measurement involves the procedure, best known as inversion, in which we assume that we know the operating principle of our measurement system well enough to model it in such a way that we can predict how it will reproduce the ambient size distribution. Mathematically, the ambient size distribution, with n size bins, is represented by the row vector $\boldsymbol{A}$, the measured size distribution, with m size bins is represented by the column vector, $\boldsymbol{M}$, and the $n \times m$ matrix, $\boldsymbol{T}$, is a probabilistic description of how the instrument will actually measure a particle of size i. Stated differently, the matrix $\boldsymbol{T}$ describes the probability that a particle in size element i will actually be put into size element j, where $j < i$. The relationship between $\boldsymbol{A}$ and $\boldsymbol{M}$ is expressed in the relationship:

$$M = \mathbf{T}A \tag{1}$$

This can be solved analytically by multiplying both sides of Eq. (1) by the inverse of $\mathbf{T}$, $\mathbf{T}^{-1}$, i.e.

$$\mathbf{T}^{-1}M = \mathbf{T}^{-1}\mathbf{T}A = A \tag{2}$$

This, however, can only be done if the inverse of **T** can be calculated, an operation that usually is not possible in problems such as the one being posed in this application. The alternative solution is to implement an iterative process in which we propose a value for the ambient distribution, calling it A^*, multiply it by our transformation matrix, **T**, and obtain a size distribution, M^*, that we compare with our measured distribution, **M**. If $M^* = M$, then $A^* = A$. Otherwise we need to adjust our value of A^* and recalculate M^*. We continue this iteration until we get an M^* that is a reasonable approximation to **M**, where reasonable approximation means that the difference between the two vectors is within a preset value.

In order to converge on the best estimate of **A**, we need an efficient method for making the first guess of A^* and adjusting each subsequent guess. There are a number of problems that must be addressed when implementing an inversion algorithm, for example there may not be a single size distribution that can produce what is measured, the iterative process might converge on a solution that produces a physically unrealistic distribution or our model of the system might not be sufficiently accurate. The inversion methodology is the subject of numerous articles and books related to deriving atmospheric properties from remote sensors like satellites and other types of multi wavelength photometers. Probably the best known methodology in the atmospheric sciences is that described by Twomy (1977) for the inversion of multi wavelength satellite measurements to obtain the properties of aerosols. To derive the size distribution measured by the BCP we have selected a modified version of the Twomy algorithm developed by Markowski (1987).

The BCP creates the measured size histogram with m channels spanning a nominal optical diameter range from 5 μm to 75 μm, over fixed time intervals. The thresholds of the size bins are related to the peak measured voltage of the particles and are selected so that the width of the bins are approximately equal with respect to the optical diameter of the particles. The firmware in the BCP decides into which bin the particle's peak voltage should be classified and increments the bin by one so that at the end of the

time interval there is a frequency distribution of the number of particles counted per size interval. This is the measured distribution, **M**.

In order to create the transformation matrix, **T**, not only do we need the probability distribution that predicts which fraction of the particles that fall in bin j should have ac-
5 tually been placed in bin l, as a result of the Gaussian intensity distribution of the laser beam, we also have to take into account that some particles with different sizes have the same scattering cross section due to the light scattering properties. As illustrated in Fig. 5, the scattering cross section, calculated here with Mie theory (Mie, 1908), does not increase monotonically with diameter. When the BCP measures the light scattered
10 by particles in some size ranges, they will be classified in smaller size intervals, as shown in Fig. 5 by the horizontal line that crosses two diameters 3.0 and 3.5 µm that have the same scattering cross section. This response must also be modeled and included in the transformation matrix.

There are other properties of cloud particles that further complicate the derivation of
15 size distribution, for example non-spherical ice crystals will scatter light quite differently although their geometric size might be approximately the same as a water droplet of equivalent diameter. Although these properties could be included in the matrix, **T**, at present we derive the transformation matrix only for the case of spherical particles with a refractive index of 1.33, i.e. that of water.

20 The transformation matrix for an individual BCP is generated by stepping through 85 diameters, in 1 µm steps, from 5 µm to 90 µm, calculating the scattering cross section with Mie scattering theory, then multiplying by the intensity map of the laser beam, where the highest intensity is set to unity, in order to determine in which size cells, j, a particle of size, l, will fall. This produces a **T** matrix that is 85 rows by m columns.
25 Figure 6 shows the probability distributions for particles with optical diameters 10, 20, 30 and 40 µm. What is shown is the probability that a particle with the given diameter will actually be classified into a smaller size category. For example, the 40 µm particle has the highest probability of being put into the 12 µm size category. Some fraction of the 40 µm particles will also be classified as other diameters between 12 and 40 µm.

The Backscatter Cloud Probe

K. Beswick et al.

Title Page

Abstract | Introduction

Conclusions | References

Tables | Figures

|◄ | ►|

◄ | ►

Back | Close

Full Screen / Esc

Printer-friendly Version

Interactive Discussion

As an example of how the measurement with the BCP is a distortion of the ambient distribution, Fig. 7 illustrates how a hypothetical size distribution, *A*, would be measured by the BCP if the measurement principle and Mie scattering are correctly modeled. In this figure, a theoretical, Gaussian size distribution, *A*, is generated then multiplied by the transformation matrix, **T**, to calculate the hypothetical *M*. The three curves in blue, green and magenta illustrate simulated size distributions assuming 90, 30 and 10 channels, respectively, in the BCP. In the following section we explore the factors that relate to the accuracy of the inversion, as well as other sources of uncertainty in the interpretation of measurements from the BCP.

2.4 Error analysis

The BCP's primary function when it was designed was to identify the presence of cloud. Here we define a cloud in terms of optical depth that can be derived from the extinction coefficient, B_{ext}, which is approximated from the measured size distribution.

$$B_{ext} = \pi \Sigma \theta_{ext} N(d_i) d_i^2 \cong \pi 2 N_T d_a^2 \tag{3}$$

Where θ_{ext} is the extinction efficiency at a given wavelength, diameter and refractive index and $N(d_i)$ is the number concentration of cloud particles with an optical diameter of d_i. For optical diameters much larger than the incident wavelength, as will be the case for the measurements with the BCP whose laser wavelength is 680 nm, the extinction efficiency is approximately two and we can estimate the extinction coefficient with Eq. (3), i.e. $B_{ext} = \pi 2 N_T d_a^2$ where N_T is the total number concentration and d_a is an area equivalent diameter.

Studies of cirrus in the last 10 yr have led to the categorization of sub-visible clouds as those with optical depth, τ, less than 0.03 (Sassen et al., 1989). Since the BCP's first mission is on commercial airliners whose cruise altitude is at temperatures where only cirrus will be found, we will use 0.03 as an operational definition to calculate the concentration of cloud particles that we expect the BCP to be able to detect. The optical

depth is defined as the average extinction coefficient multiplied by the average cloud layer, ΔZ:

$$\tau = B_{ext}\Delta Z \cong \pi 2 N_T d_a^2 \Delta Z \tag{4}$$

Under the assumption of an average, area equivalent diameter d_a and cloud depth, ΔZ, we can determine the number concentration that will produce a cloud with $\tau = 0.03$. For example, thin cirrus have effective diameters in the range from 30–40 µm (e.g. Gayet et al., 1996), so if we choose $d_a = 40$ µm and use a conservative value for $\Delta Z = 100$ m, then $B_{ext} = 3 \times 10^{-6}$ cm^{-1} and $N_T = 0.03$ cm^{-3}. Hence, we need to estimate the uncertainty in measuring the total concentration so that we can determine the accuracy with which the BCP can meet its original objective.

The concentration is determined by counting the number of cloud particles detected within the size range of the BCP over a selected time period and dividing by the volume of air, V, which passes through the sensitive sample area, SA. The volume of air is calculated as

$$V = SA \cdot AS \cdot T \tag{5}$$

Where AS is the airspeed at the BCP sample area and T is the sampling time. The counting efficiency of the BCP is 100 % as long as there are no coincident particles in the beam since these would be counted as a single particle. Given the very small sample area of the BCP this is a very low probability event unless concentrations exceed 500 cm^{-3}.

Hence, the source of most of the uncertainty associated with deriving the number concentration is in the determination of SA and AS. The SA, as previously discussed, is measured with the droplet mapping system that has a linear position accuracy of ±10 µm, which means that the area is estimated with a root sum square (RSS) accuracy of ±14 µm^2, or ±8 % for the BCP with measured sample area of 0.18 mm^2. This accuracy estimate is a good approximation for the case of the 22 µm droplets that were used to map the area because, even near the edges of the beam where the intensity

is only 15 % of the maximum intensity, the scattered light will still exceed the minimum detection threshold. Thus, droplets 22 μm and larger will have a sampling area of $0.18 \pm 0.014\,\text{mm}^2$.

When we look at the scattering cross sections generated by our Mie calculations,
5 and shown graphically in Fig. 5, we see that a particle with optical diameter of 5 μm, the current lower size limit of the BCP, has a scattering cross section of $0.7 \times 10^{-8}\,\text{cm}^2$ so that if a particle passes through the least intense part of the beam and scatters less than this, it will not be detected and hence the effective sample area for that particle will be less than for the 22 μm particle. Dividing $0.7 \times 10^{-8}\,\text{cm}^2$ by 0.15 results in a scattering
10 cross section of $4.6 \times 10^{-8}\,\text{cm}^2$, the scattering cross section through which a particle would have to pass and still scatter sufficient light to be detected. In looking at Fig. 5 (and looking up the value in the data file for this figure) we see that particles > 15 μm meet this criterion and particles smaller than this size have decreasing sample area.

The transformation matrix actually takes these differing sample areas into account
15 because the creation of the probability matrix requires that some fraction of the particles smaller than 15 μm will go undetected and the entries in the matrix corresponding to what fraction of a measured size are actually from larger diameters reflect these losses. The reconstructed ambient distribution that results from the inversion will accurately reflect both the shape and concentrations in the size channels as long as the
20 majority of the particles are larger than 15 μm. As will be further elaborated below, the inversion does not recover 100 % of the ambient distribution in sizes smaller than 15 μm; however, these losses are compensated by multiplying their concentrations, after the inversion, by the ratio of the total sample area for particle larger than 15 μm to the effective sample area for each of the particles with diameters less than 15 μm. For
25 example, the sample area for a 10 μm particle is $0.12\,\text{mm}^2$ so the correction factor is 1.5.

The air speed at the sample area is the other variable needed to calculate the sample volume. The sensitive region of the BCP is 4 cm from the skin of the aircraft; hence, the velocity of the particles at this point may be slower than the free airstream. On the

The Backscatter Cloud Probe

K. Beswick et al.

Title Page

Abstract | Introduction

Conclusions | References

Tables | Figures

|◀ | ▶|

◀ | ▶

Back | Close

Full Screen / Esc

Printer-friendly Version

Interactive Discussion

other hand, aircraft airspeed sensors are 6 cm from the skin, so if we use the measured aircraft speed in our calculations, we are likely to be within 20 % of the actual airspeed at the sample volume. As will be demonstrated in Sect. 3.1, comparison with other cloud spectrometers indicate that this assumption is valid. In summary, the accuracy in the measurement of the number concentration is dominated by the uncertainty in the airspeed. This means that the cloud detection threshold previously stated as 0.03 cm^3, can be measured within a factor of ±20 %.

The other factor to take into account when estimating the concentration is the amount of time required to obtain a statistically significant sample. Using Poisson sampling theory, in order to be confident that the sample is representative of the general particle population, at least 100 particles must be measured in order to have a uncertainty less than 10 % ($n^{1/2}/n$). To measure a concentration of 0.03 cm^{-3}, the approximate concentration of a thin cirrus with an optical depth of 0.03, a volume 3000 cm^3 must be sampled. The BCP discussed in this paper has a sample area of 0.18 mm^2 and a commercial airliner flies at an airspeed of approximately 250 m s^{-1}. This means that 45 cm^3 s^{-1} of air is sampled and measurements would need to be accumulated over approximately 60 s to get a statistically relevant value. If a 20 % uncertainty is acceptable, then only 25 particles are needed and the sampling time is reduce to 15 s.

The accuracy with which the ambient size distribution is retrieved by the inversion is a function of three factors: (1) the number of channels in the measured size distribution, (2) the fraction of the ambient size distribution with concentrations in optical diameters smaller than about 15 μm, and the width of the ambient distribution. The accuracy depends upon how much of the original information contained in the ambient distribution is maintained during the measurement process. Even though particles are being undersized over a range of values as they go through the sample area in uniformly, random locations, if they are placed in a smaller size bin whose width is very small, then the new size has retained most of the original information, i.e. if a 20 μm particle gets sized some fraction of the time as a 10 μm particle, and the width of the channel for 10 μm particles is only 1 μm, then the inversion will put that particle back

The Backscatter Cloud Probe

K. Beswick et al.

Title Page

Abstract | Introduction

Conclusions | References

Tables | Figures

|◄ | ►|

◄ | ►

Back | Close

Full Screen / Esc

Printer-friendly Version

Interactive Discussion

into the 20 µm bin. However, if the width of the measured distribution channels is 5 µm, then information is lost when the 20 µm particle gets sized as a 10 µm particle but in the process of re-binning it is placed in a channel that might also contain 7, 8, 9, 10, 11, and 12 µm particles. In this case, the inversion will be unable to produce as accurate of a representation of the ambient distribution since 7–12 µm particles can end up in the size bins around the 20 µm size bin of the retrieved distribution. The subsequent effect is a retrieved distribution that is broader than the ambient. Figure 7 illustrates how the simulated measured size distribution appears when the data are binned in 10, 30 and 90 channels.

The importance of the fraction of particles smaller than 15 µm in the ambient distribution and how they impact the retrieval accuracy is that, in the case of the BCP whose sample area was evaluated above, these smaller particles will be lost as they go through the edges of the beam where particles > 15 µm were undersized but not lost. As discussed above, this is partially compensated by adjusting the sample areas after the inversion; however, information from the ambient distribution is lost from the small particle sizes that cannot be completely retrieved since we do not know a priori what the shape of the ambient distribution will be.

The third parameter that limits the accuracy of the retrieval is the width of the ambient size distribution. This is also an issue of information loss. The most rigorous test of a retrieval is that of a monodispersed particle distribution whose measured distribution would look similar to one of the probability distributions that were shown in Fig. 6 if the channels of the measured distribution have very narrow widths so as to capture the detailed structure of the many possible measured sizes. Due to the finite widths of the measured distributions, however, these structures are smoothed out so that the subsequent inversion produces a retrieved distribution broader than monodispersed. When the ambient distribution is broader, the resultant distribution that is measured is the mixture of probabilities that also smooth the intrinsic shape of the probability distributions, but the retrieval then is able to better reproduce the broader ambient distribution. This is illustrated in Fig. 8 where the ambient distribution is simulated with

Title Page

Abstract | Introduction

Conclusions | References

Tables | Figures

|◄ | ►|

◄ | ►

Back | Close

Full Screen / Esc

Printer-friendly Version

Interactive Discussion

a Gaussian probability function with a constant concentration and average diameter of $100\,cm^{-3}$ and $20\,\mu m$, respectively and the standard deviation is set to $2\,\mu m$, $6\,\mu m$ and $10\,\mu m$. The black curves are the simulated ambient distributions, the green curves are the simulated "measured" distributions assuming a 90 channel simulated "measured"
distribution. The simulated "measured" distribution is similar to that illustrated in Fig. 6 where the simulated ambient distribution is multiplied by the transformation matrix. The blue and red curves show the simulated ambient and "measured" distributions following application of the inversion.

Figure 9 shows the result of evaluating a range of simulated ambient and "measured" size distributions, varying the number of channels of the simulated measured distributions, the average diameter and the standard deviation of the distribution in order to evaluate the accuracy of the retrieval with respect to the three factors discussed above. The error is calculated as the average squared difference between the simulated and retrieved ambient distributions. In this figure we see that regardless of average diameter and number of channels in the simulatedmeasurement, the error decreases exponentially in most cases with increasing standard deviation. The second observation is that increasing the number of channels in the measurement decreases the error significantly. The increasing of the average diameter, i.e. moving the majority of the particles to sizes larger than the threshold size, also decreases the error but the largest error is when measuring with a small number of size channels.

3 Flight results

Several BCPs have been flying on commercial aircraft since September 2011. Prior to being mounted on these aircraft the BCP was flown on research aircraft in order to evaluate its performance in comparison with other spectrometers that are routinely used in cloud research to measure size distributions. We describe one of these flight evaluations in Sect. 3.1 then show some results in Sect. 3.2 from the BCPs that are currently flying on the commercial aircraft

The Backscatter Cloud Probe

K. Beswick et al.

3.1 Measurements on the BAE-146

The BCP has been evaluated by comparing its measurements with commercial, optical particle spectrometers during flights on the BAE-146 operated by the FAAM. The measurements on the BAE-146 were made in September 2010 in flights over the North Atlantic as part of the IAGOS-DS, and Septex Cloud-Radiation projects (http://www.faam.ac.uk/index.php/home). Flights were made through a range of cloud types and temperatures from which one example is highlighted here. As was previously shown in Fig. 3a, the BCP was mounted on the forward, starboard window-blank #3 located $\sim$ 5 m from the aircraft nose upstream of the aircraft's Johnson–Williams hot-wire total liquid water content probe. In addition to the BCP, there were other cloud microphysical optical spectrometers flown, including the DMT cloud droplet probe (CDP) that has been described by Lance et al. (2010) and a cloud and aerosol spectrometer (CAS) first introduced in the year 2000 (Baumgardner et al., 2001). The CDP, CAS and other 2-D optical array probes were mounted on the aircraft wing pylons within the free air stream. These probes should not be subject to distortions of the free-stream ambient particle size distributions due to fuselage induced streamline compression. This effect is described in greater detail in the discussion section.

Figure 10a shows a time series of number concentrations from the BCP, CDP and CAS during a four hour flight (B553 using the FAAM research flight designation, conducted in September 2010). Also shown with the green curve is the ambient air temperature. Figure 10b is a time series of the same variables but over the time period 35 000–37 000 UTC seconds of the day when the aircraft was penetrating an all water cloud. We choose this particular time period for comparing the three instruments to avoid potential artifacts caused by the fragmentation of ice crystals on aircraft or instrument leading edges (see the discussion section for more detail on this aspect of the measurements).

The CAS measures in the size range from 0.5 to 50 µm, the CDP measures from 2.0 to 50 µm and the BCP from approximately 5 to 60 µm; hence, the higher concentrations

measured by the CAS are expected since it will be measuring some of the accumulation mode aerosol in addition to the water droplets. In general the BCP tracks the changes seen in the CDP and CAS data over almost two orders of magnitude (1–300 cm^{-3}).

The effect of aircraft attitude, i.e. its yaw angle, might be seen in the periods when the BCP concentration is observed to exceed that of the CDP and almost reaches that of the CAS, such as at 35 800 and 35 900, then falling below the CDP at 35 850 and 35 950. Changes in the yaw angle will lead to accelerations and decelerations of the air passing through the BCP sample volume, leading to increases and decreases in the concentration, respectively, since we are assuming a constant airspeed. As we don't have the aircraft attitude data available at this time, the explanation for this oscillation of BCP concentration remains only speculation. It does, however, underscore one of the uncertainties that must be taken into account when interpreting the measurements from the BCP and the need for data quality control.

Figure 11a and b show the time series of liquid water content (LWC) and median volume diameter (MVD) for the same time periods as shown in Fig. 10b in the all liquid cloud. This comparison evaluates the accuracy of the sizing by the BCP where even small deviations with respect to the MVD of the CAS and CDP will become amplified due to the diameter cubed sensitivity of the LWC calculation. Both the LWC and MVD time series shows that the BCP is in very good agreement with both the CAS and CDP. Even though the CAS is measuring to smaller sizes than the BCP or CDP, the diameter cubed sensitivity of LWC and MVD minimize the contribution of the sub-micron particles.

As a final method to evaluate how well the BCP measures cloud droplets in relationship to the CDP and CAS, the size distributions measured by the CAS and CDP were averaged over the cloud pass from 35 500 to 36 600 and compared with the average size distribution, over the same period, that was extracted from the BCP measurements by the inversion method described in Sect. 2.3. The CAS and CDP have 30 channel size distributions whereas the BCP has only 10 channels; however, to demonstrate how we can create a larger number of channels with the inversion, we also show the

retrieved 90 channel distribution. As seen in Fig. 12 the inversion does a reasonable job of capturing the peak and width of the size distribution when compared to the other two spectrometers.

3.2 Results from the BCP on commercial aircraft

As previously mentioned in the introduction, the BCP was originally designed as a compact and robust detector for cloud particles as part of the IAGOS program. After one of the BCP prototypes underwent the evaluation on the BAE-146 in February and March of 2011, two operational units were delivered to the IAGOS management team for installation on a Lufthansa A340-300 "Viersen" airliner in May 2011, along with the rest of the IAGOS instrument package. The BCP was mounted next to the inlets for the aerosol and gas analyzers as shown by the photograph in Fig. 13.

The first test flight of the Viersen with this instrument package occurred in July 2011 and routine operation began in September 2011. A second IAGOS instrument package was installed on a China Airlines Airbus-340 "B-18806" on 26 June 2012, and commenced routine operations in January 2013. Both aircraft are currently flying international routes as of the submission of this manuscript.

As of March 2013, the BCP had taken data on a total of 1211 flights, representing 7357 h of flight time during which 340 of those hours had been in cloud, where a cloud encounter is defined as more than 20 s. Figure 14 summarizes the trajectories of all the flights for the 18 months covering the first of September 2011 to the end of March 2013. The colored, filled circles along the flight track indicate where clouds were encountered and the color scale shows the number concentration. The yellow diamonds are points of arrival and departure of the aircraft. Note that the concentrations are given in units of number per cubic centimeter.

Table 1 summarizes some of the general statistics with respect to the regions that were covered by the flights: (1) the number of flights, (2) the hours of flight time, (3) the total number of hours in cloud, (4) the fraction of flight hours in which the aircraft

was in cloud, (5) the fraction of flights that encountered clouds at normal cruise altitude (9–11 km), (6) the fraction of takeoff through clouds and (7) the fraction of landings through cloud.

Figures 15 and 16 are expanded views of the flights between Europe and North America and Europe and South America, respectively. These two regions are highlighted because flights covering these regions are the longest in duration and 70 % of these flights also encountered clouds at cruise altitude. More than 90 % of the flights from Frankfurt to Rio encountered clouds at cruise altitude. The Asia routes (not shown here), although somewhat shorter in duration, also encountered clouds at cruise altitude during more than 70 % of the flights. The importance of these types of data and implications for climate and flight safety are examined further in the next section.

4 Discussion

As previously explained in the introduction, the BCP was originally designed to be a cloud/no cloud indicator but DMT included in the development the possibility to also provide some information regarding the effective optical diameter (EOD), i.e. the diameter that a spherical water droplet would have if it scattered the measured amount of light. The derivation of the EOD is complicated by the Mie scattering ambiguities and the non-uniform incident laser intensity that required an inversion of the data to derive and estimated EOD. The comparison of the derived, inverted size distribution from the BCP, and the LWC and MVD with the more traditional cloud probes (Sect. 3.1) showed that the agreement was quite good, considering the assumptions that go into the inversion.

Expanding upon the error analysis in Sect. 2.4, one uncertainty when interpreting the measurements is that of the airflow velocity distribution at the sample volume of the BCP. The viewing volume of the BCP is likely within the boundary layer. There have been numerous modeling and observational studies of airflow effects on particle

measurements all of them showing that the airspeed decreases as you approach the skin of the aircraft and, in addition, the compression of the streamlines leads to the size sorting as particles less than 20 µm tend to follow the streamlines whereas larger droplets partially cross them. The subsequent effect is that particles larger than 20 µm can appear to have concentrations larger than their ambient values so that they are overestimated. For example, Twohy and Rogers (1993) show that droplets with diameters of 50 µm are enhanced by a factor of two over ambient. The interested reader can find more in the articles by King (1984), King et al. (1984), Norment (1988), and Twohy and Rogers (1993). We assume that the airspeed in our calculations is the same as measured for the aircraft to derive the concentrations on the Airbus 340-300 aircraft, but since we have nothing to compare with, nor do we have measurements of the airspeed at that point, the uncertainty could be as much as ±20 %. Likewise, without doing the airflow modeling such as has been done for various research aircraft to locate optimum mounting positions for cloud probes, we don't know what type of enhancements might be occurring in the concentrations at various aerodynamic diameters. At some locations on the aircraft there can also be a "shadow zone" where the boundary layer has grown to a thickness sufficient to carry cloud particles outside of the sensing volume of an instrument. This is apparently not the case for either the measurements on the BAE-146 or the Airbuses given that the BCP is detecting cloud particles.

Ice crystal shattering is another source of uncertainty and measurement error. A number of studies have highlighted the issue of ice crystals shattering and water droplets splattering on the leading edges of instruments (e.g. Engblom and Ross, 2003; Korolev et al., 2013), leading to artificially created particles that confound the measurements. The geometry of the BCP, i.e. lack of any leading edges for droplets or crystals to impact and break means that the instrument itself will be free of probe-induced artifact; however, the fuselage of the aircraft provides a large surface for cloud particles to strike and shatter into smaller fragments. The results from the BAE-146 discussed in Sect. 3.1 were for warm clouds and there might have been splashing but the time series of the concentrations (Fig. 10b) don't seem to indicate any systematic bias. When

looking at cold clouds, however, when temperatures were lower than −10°C, we see a possible bias in concentrations measured by the CAS and BCP, as seen in Fig. 17. The CAS is known to have shattering issues when a sufficient number of large ice crystals are present (Heymsfield, 2007; McFarquhar et al., 2007), and in this case it
5 is showing concentrations 100 times higher than the CDP, an open path instrument. These are too high to be aerosol particles. The BCP is also measuring concentrations in the same range as the CAS. Although it could be that the CDP is for some unknown reason not seeing as many ice crystals as the CAS and BCP, the more likely explanation is the crystal breakup on the CAS inlet and on the aircraft fuselage ahead
10 of the BCP. The sometimes large concentrations seen in the BCP measurements on the Airbus are likely the result of enhancement due to crystal break-up since temperatures are always lower than freezing at the cruise altitude and cirrus crystals, although usually rather small at very cold temperatures, can still sometimes reaches sizes large enough to fracture on impact. Although this introduces a large error in the concentration
15 reported, as we discuss below, such high ice crystal concentrations can also impact other sensors on the aircraft.

The comparison of the BCP with the CDP and CAS on the BAE-146 was encouraging, from two aspects: (1) the number and mass concentrations compared well with respect to the general tendencies over the whole flight and (2) the size distributions
20 were in good agreement with respect to peaks and shapes. This gives us confidence that a measurement so close to the aircraft skin can give a reasonable representation of the cloud properties with minimal distortion due to airflow and that the inversion technique is robust enough to extract size information.

The preliminary analysis from the BCPs that are part of the IAGOS package on the
25 Airbus aircraft shows that there is an abundance of cloud data and a wealth of information that can be extracted on cloud microphysical properties in the size range of the BCP as long as caution is taken when ice shattering may be a potential source of artifacts. A detailed analysis of these data is well beyond the scope of this paper that is mostly focused on the technical aspects of the BCP. That being said, a cursory look at

some of the regions of the world where desert dust and clouds are encountered offer a tantalizing hint of the types of information that can be obtained that will give us a data set that can be used to compare with satellite measurements and to validate climate and cloud/dust models. Looking at Fig. 16, the flight trajectories from Frankfurt to Rio de Janeiro, we see that there are many clouds and quite a few with concentrations greater than $1\,cm^{-3}$. This is not an insignificant concentration of ice crystals when we convert this to units normally used when describing ice crystal populations, i.e. number per liter. More than a $1000\,L^{-1}$ is an enormously high concentration of ice crystals for cirrus, the type of cloud that would normally be found at these altitudes and temperatures. If some of these penetrations are through the outflow of deep convection, then such concentrations might be found. It is more likely that the ice crystal concentration is being multiplied by breakup on the fuselage. From the point of view of better understanding ice cloud microphysics, these high, artificial concentrations obscure some of the important features of these clouds; however, from the viewpoint of aircraft flight operations, the high concentrations are potential hazards as these crystals and their fragments are the very type of cloud particles that have been documented as obstructing inlets to temperature sensors and pitot tubes that measure air speed. That these measured high concentrations are found not only over the same route where documented aircraft incidents have happened, but over many other regions of the world highlights the importance of having this type of information available in real time for flight crews to make informed decisions.

Finally, the vertical structure of clouds is also an important measurement and each flight has vertical profiles during takeoff and landing. As shown in Table I, 50 % of the take offs and 55 % of the landings encountered clouds, i.e. more than 600 vertical profiles of cloud structure are currently in the data base. These are data that can be used to compare with radar, lidar and satellite measurements, as well as providing useful climatology for use in climate and weather forecast models. Figure 18 illustrates one such example of cloud structure as the aircraft was landing at the Frankfurt airport. Figure 18a shows the vertical structure of the number concentration and Fig. 18b shows

how the MVD varied. As shown by the horizontal red lines, there were four distinct layers over an altitude range of 2000 m, as indicated by the number concentration (Fig. 18a).

5   Summary and conclusions

A compact, lightweight single particle cloud spectrometer, the Backscatter Cloud Probe (BCP) is described that operates autonomously and measures the number concentration of particles in the equivalent optical diameter (EOD) range nominally from 5–75 µm. The BCP, originally designed solely as an indicator of the presence of cloud for use in quality control for measurement with the European Union In-Service Aircraft for a Global Observing System (IAGOS) package, provides a measurement of EOD and retrieves size distributions from the ambient size distribution with an inversion technique.

The sizing and sample area of the BCP has been calibrated in the laboratory using a monodispersed droplet stream (Lance et al., 2010), compared with other cloud particle spectrometers on research aircraft and is now flown operationally on two commercial aircraft flying international routes.

The comparison of the BCP with two other spectrometers, the CDP and CAS, show that the BCP, whose active sample volume is only 4 cm from the aircraft skin, compares very well in number concentration and size distributions with the other two spectrometers.

The BCPs on two commercial airliners, Lufthansa and China Airlines Airbus 340–300s, have taken more than 7000 h of data during more than 1200 h of flight time. At cruise altitude between 9 and 11 km, 40 % of the flights encountered cirrus and 50 % of the take offs and landing were made through cloud layers. The 340 total hours of cloud data and more than 600 vertical profiles through cloud are a valuable data base of information that provide measurements that can complement those from remote sensors like radar, lidar and satellites, as well as being useful for validating algorithms

The Backscatter Cloud Probe

K. Beswick et al.

Title Page

Abstract | Introduction

Conclusions | References

Tables | Figures

|◀ | ▶|

◀ | ▶

Back | Close

Full Screen / Esc

Printer-friendly Version

Interactive Discussion

for extracting microphysical properties from remote sensing measurements. As with data from any cloud spectrometer in conditions of high ice concentration, care must be taken to eliminate any data sets where ice shattering on the fuselage may produce artifacts in the measurements.

In addition to the value for research on cloud properties, the data also provides important information to the aircraft industry on statistics related to the frequency of flight encounters with high ice crystal concentrations, events that pose potential hazards to flight operations.

References

Baumgardner, D., Jonsson, H., Dawson, W., O'Connor, D., and Newton, R.: The cloud, aerosol and precipitation spectrometer (CAPS): a new instrument for cloud investigations, Atmos. Res., 59–60, 251–264, 2001.

Baumgardner, D., Chepfer, H. Raga, G. B., and Kok, G. L.: The shapes of very small cirrus particles derived from in situ measurements, Geophys. Res. Lett., 32, L01806, doi:10.1029/2004GL021300, 2005.

Engblom, W. A. and Ross, M. W.: Numerical Model of Airflow Induced Particle Enhancement for Instruments Carried by the WB-57 Aircraft. NASA Aerospace Report No. ATR-2003(5084)-01, 29 pp., 2003.

Field, P. R., Heymsfield, A. J., and Bansemer, A.: Shattering and particle interarrival times measured by optical array probes in ice clouds, J. Atmos. Ocean. Tech., 23, 1357–1370, 2006.

Gayet, J. F., Febvre, G., Brogniez, G., Chepfer, H., Renger, W., and Wendling, P.: Microphysical and optical properties of cirrus and contrails: cloud field study on 13 October 1989, J. Atmos. Sci, 53, 126–138, 1996.

Heymsfield, A. J.: On measurements of small ice particles in clouds, Geophys. Res. Lett., 34, L23812, doi:10.1029/2007GL030951, 2007.

King, W.: Air flow and particle trajectories around aircraft fuselages, I: Theory, J. Atmos. Ocean. Tech., 1, 5–13, 1984.

King, W., Turvey, D., Williams, D., and Llewellyn, D.: Air flow and particle trajectories around aircraft fuselages, II: Measurements, J. Atmos. Ocean. Tech., 1, 14–21, 1984.

Korolev, A. V., Kuznetsov, S. V., Makarov, Y. E., and Novikov, V. S.: Evaluation of measurements of particle size and sample area from optical array probes, J. Atmos. Ocean. Tech., 8, 514–522, 1991.

Korolev, A. V., Emery, E. F., Strapp, J. W., Cober, S. G., and Isaac, G. A.: Quantification of the effects of shattering on airborne ice particle measurements, J. Atmos. Ocean. Tech., online first, doi:10.1175/JTECH-D-13-00115.1, 2013.

Lance, S., Brock, C. A., Rogers, D., and Gordon, J. A.: Water droplet calibration of the Cloud Droplet Probe (CDP) and in-flight performance in liquid, ice and mixed-phase clouds during ARCPAC, Atmos. Meas. Tech., 3, 1683–1706, doi:10.5194/amt-3-1683-2010, 2010.

Markowski, G. R.: Improving Twomey's algorithm for inversion of aerosol measurement data, Aerosol Sci. Tech., 7, 127–141, 1987.

McFarquhar, G. M., Um, J., Freer, M., Baumgardner, D., Kok, G. L., and Mace, G.: Importance of small ice crystals to cirrus properties: observations from the Tropical Warm Pool International Cloud Experiment (TWP-ICE), Geophys. Res. Lett., 34, L13803, doi:10.1029/2007GL029865, 2007.

Mie, G.: Beiträge zur Optik trüber Medien, speziell kolloidaler Metallösungen, Ann. Phys.-Berlin, Vierte Folge, 25, 3, 377–445, 1908.

Nagel, D., Maixner, U., Strapp, W., and Wasey, M.: Advancements in techniques for calibration and characterization of in situ optical particle measuring probes, and applications to the FSSP-100 probe, J. Atmos. Ocean. Tech., 24, 745–760, doi:10.1175/JTECH2006.1, 2007.

Sassen, K, Griffin, M. K., and Dodd, G. C.: Optical scattering and microphysical properties of subvisible cirrus clouds, and climatic implications, J. Appl. Meteorol., 28, 91–98, 1989.

Twohy, C. and Rogers, D.: Airflow and water drop trajectories at instrument sampling points around the Beechcraft King Air and Lockheed Electra, J. Atmos. Ocean. Tech., 10, 566–578, 1993.

Title Page

Abstract | Introduction

Conclusions | References

Tables | Figures

◄◄ | ►►

◄ | ►

Back | Close

Full Screen / Esc

Printer-friendly Version

Interactive Discussion

Twomey, S.: Introduction to the Mathematics of Inversion in Remote Sensing and Indirect Measurements, Developments in Geomathematics 3, Elsevier Scientific Publishing Company, Amsterdam, 237 pp., 1977.

Wendisch, M., Keil, A., and Korolev, A. V.: FSSP characterization with monodisperse water droplets, J. Atmos. Ocean. Tech., 13, 1152–1165, 1996.

The Backscatter Cloud Probe

K. Beswick et al.

The Backscatter Cloud Probe

K. Beswick et al.

Table 1. Cloud Statistics from Airbus 340-300 BCP Measurements.

Region	Total flights	Total flight hours	Total time in cloud	Fraction of flight hours in cloud (%)	Fraction of flights with cloud encounters at cruise altitude (%)	Fraction of flights with cloud encounters at takeoff (%)	Fraction of flights with cloud encounters at landing (%)
Africa	85	453	34.9	7.7	62	54	61
America	128	1035	48.9	4.7	70	62	69
Asia	103	895	49.3	5.5	73	64	62
Europe	40	462	5.0	1.1	10	45	58
Far East	391	1390	53.5	3.8	24	46	53
Gulf	176	769	25.6	3.3	19	39	42
Middle East	111	462	17.2	3.7	26	42	47
Pacific	64	669	8.4	1.3	13	41	38
Rio	99	1117	97.9	8.8	94	76	80
All	1211	7357	340.	4.6	40	50	55
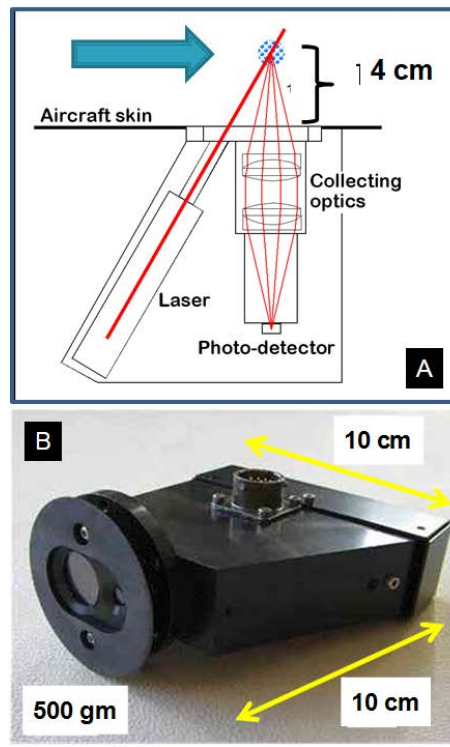
Fig. 1. The optical layout of the BCP is shown in **(a)** illustrating the principal components and the photograph of the BCP in **(b)** shows the relative dimensions of the instrument.
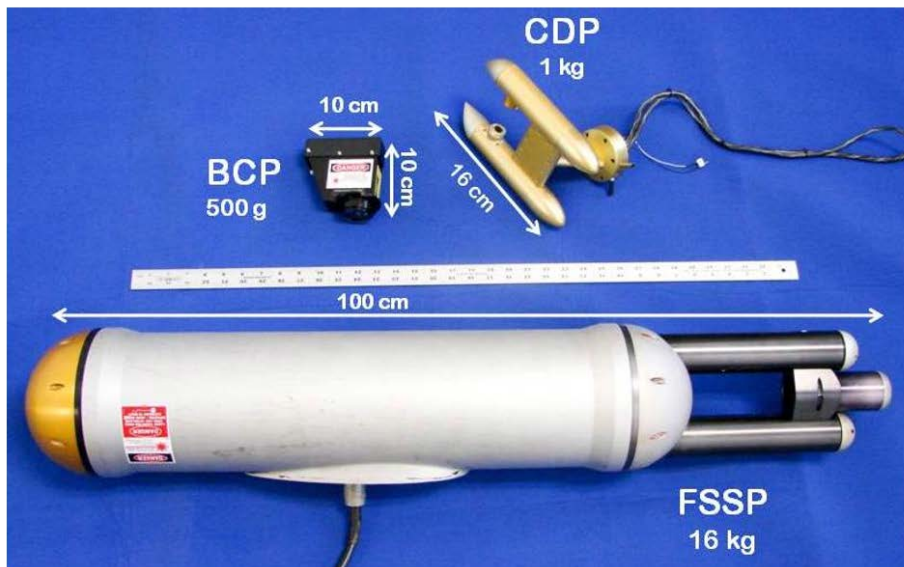
Fig. 2. In this photograph the evolution in physical size and weight is shown as the BCP is compared with the "legend" probe, the FSSP and the CDP that were introduced 40 and 10 yr ago, respectively.
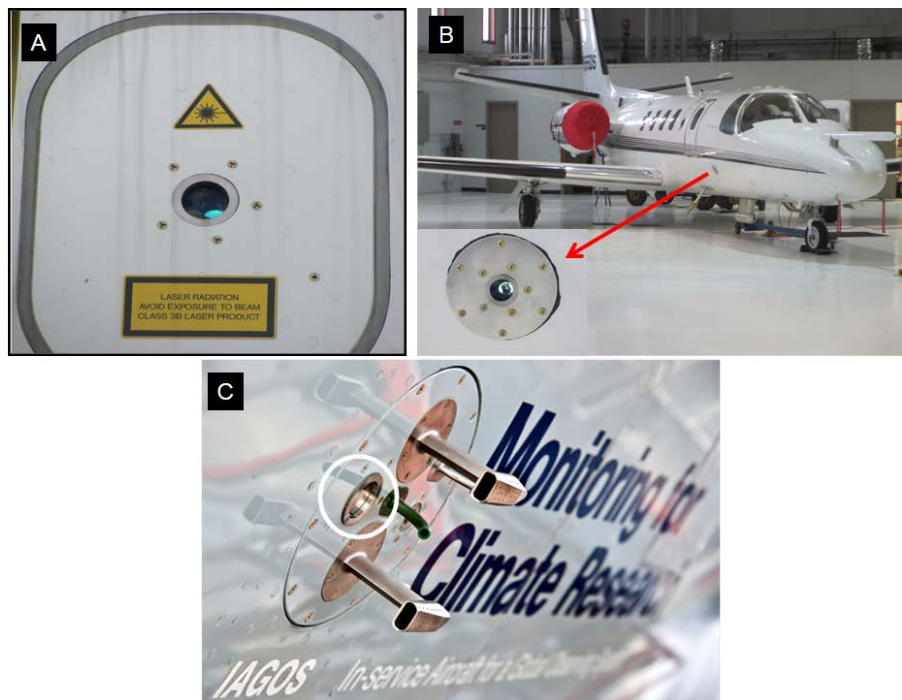
Fig. 3. The BCP is mounted with its window looking out through a transparent aperture as illustrated in these three photos: **(a)** on an access hatch of the FAAM BAE-146, **(b)** just behind and below the cockpit of the University of North Dakota Cessna Citation, inside the radio compartment and **(c)** on a Lufthansa A340-300 Airbus just behind and below the forward stairway.
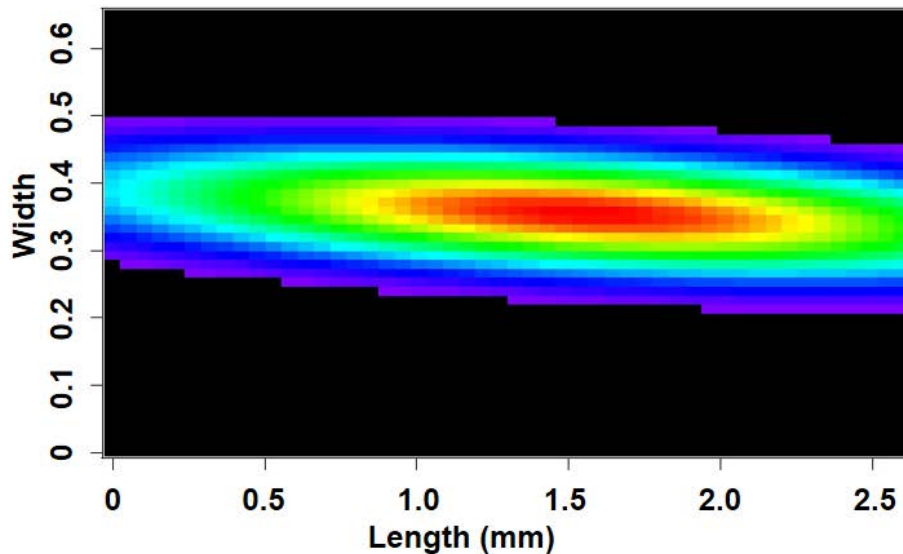
Fig. 4. The contour plot displayed here is a smoothed image of the light scattering intensity across the sensitive sample area of the BCP, mapped with 22 μm droplets with a resolution of 10 μm. The highest scattering intensities are denoted by the red color and the lowest scattering in blue.
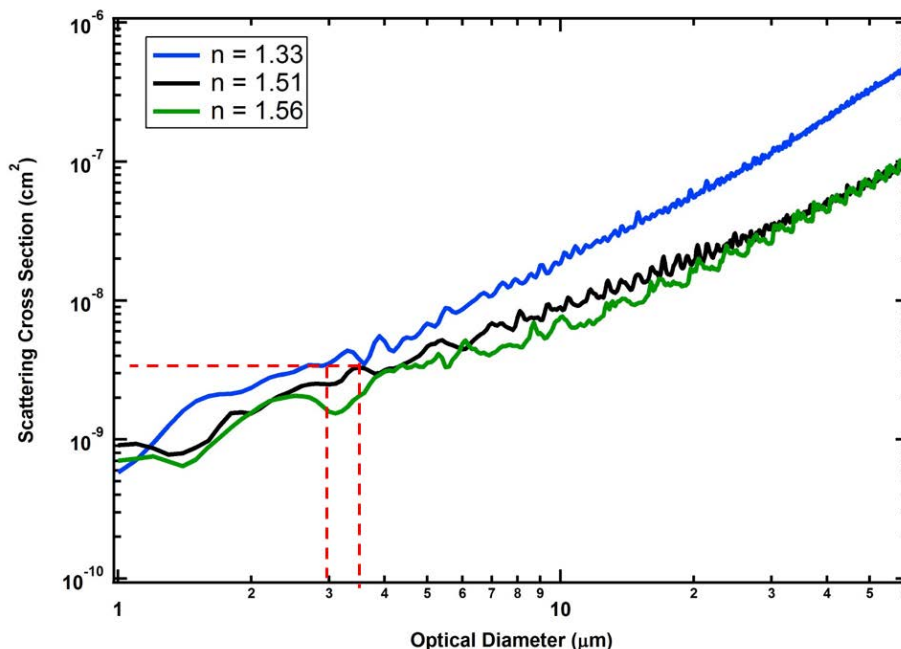
Fig. 5. The theoretical response of the BCP is shown in this diagram that relates the scattering cross section of particles to their optical diameter, calculated from Mie theory assuming spherical particles, a wavelength of 684 nm and the refractive indices for water (1.33), crown glass calibration beads (1.51) and borosilicate calibration beads (1.56). The red dashed line indicate an example where two particles with different diameter have the same scattering cross section and cannot be uniquely identified by their light scattering intensity.
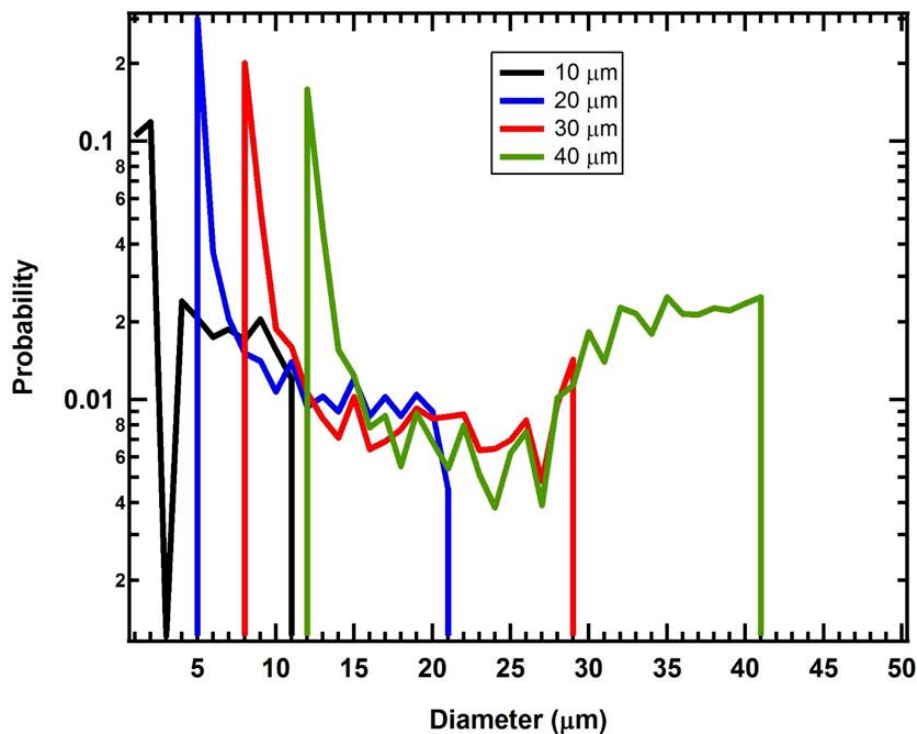
Fig. 6. This figure illustrates the theoretical probability distributions for particles with four optical diameters. The probabilities are that a particle with the given size will be measured as a particle with a smaller optical diameter. For example, a 40 μm water droplet has the highest probability of being sized by the BCP as a 12 μm droplet due to the intensity distribution of the laser beam.
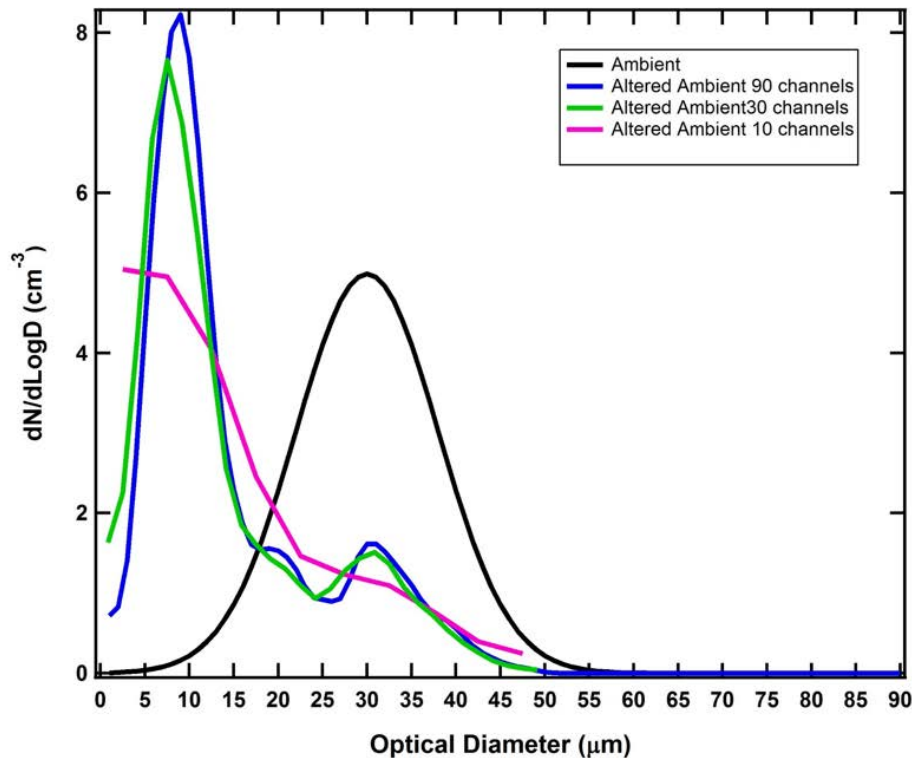
Fig. 7. The distortion of the ambient size distribution due to the measurement principles of the BCP are illustrated in this figure that shows a simulation of how the measured size distribution would appear to the BCP if the ambient distribution (black curve) was categorized into 90 (blue), 30 (green) or 10 (magenta) size bins.
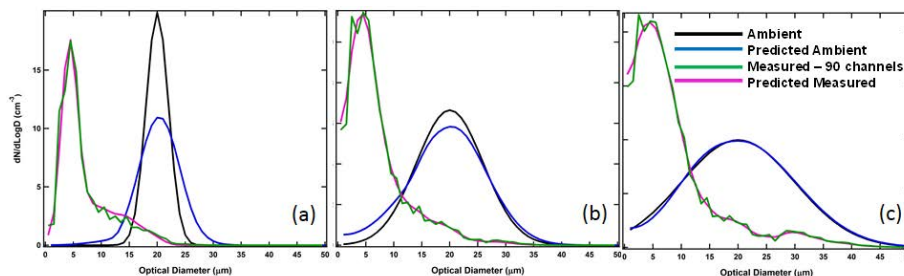
Fig. 8. The three panels illustrate how the accuracy of retrieving the ambient size distribution is related to the width of the distribution. The black curve is a simulated distribution with an average diameter of 20 µm and standard deviation of 2 µm, 6 µm and 10 µm in panels **(a)**, **(b)** and **(c)** respectively. The blue curves are the distributions retrieved from the simulated measurements shown in green and the red curve shows the predicted measurement after the inversion.
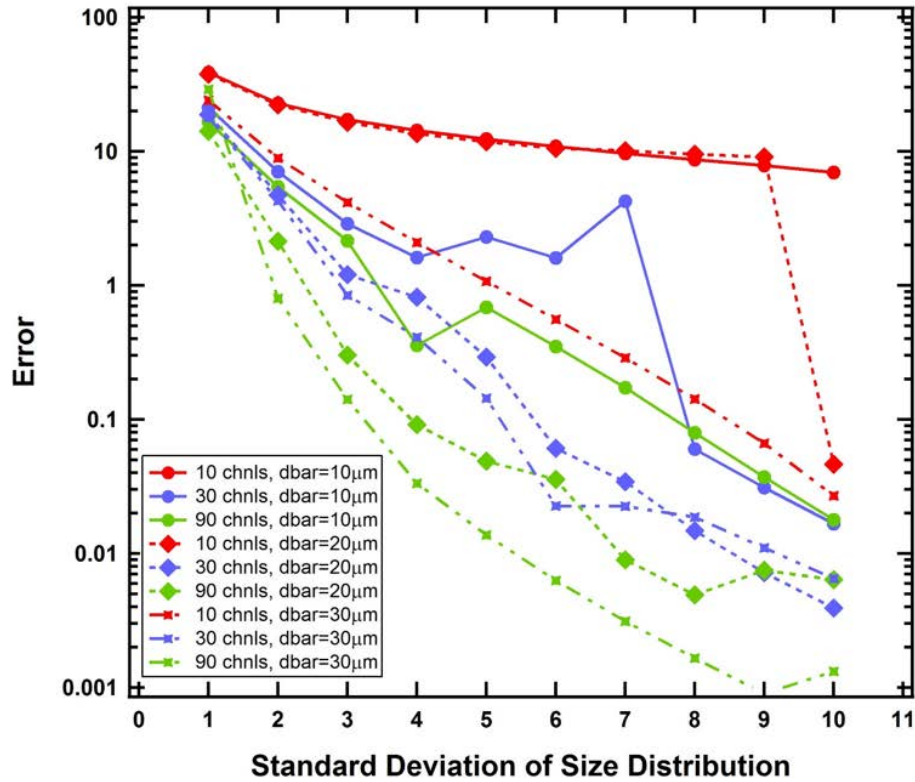
Fig. 9. The sets of curves shown in this figure illustrate the accuracy of the inversion as a function of the standard deviation of the simulated ambient (Gaussian) size distribution. Each color represents a simulated, measured size distribution binned in 10 channels (red), 30 (blue) and 90 (green). The average diameter of the simulated ambient distribution is varied from 10 μm (solid curves), 20 μm (dashed) and 30 μm (dot-dash).
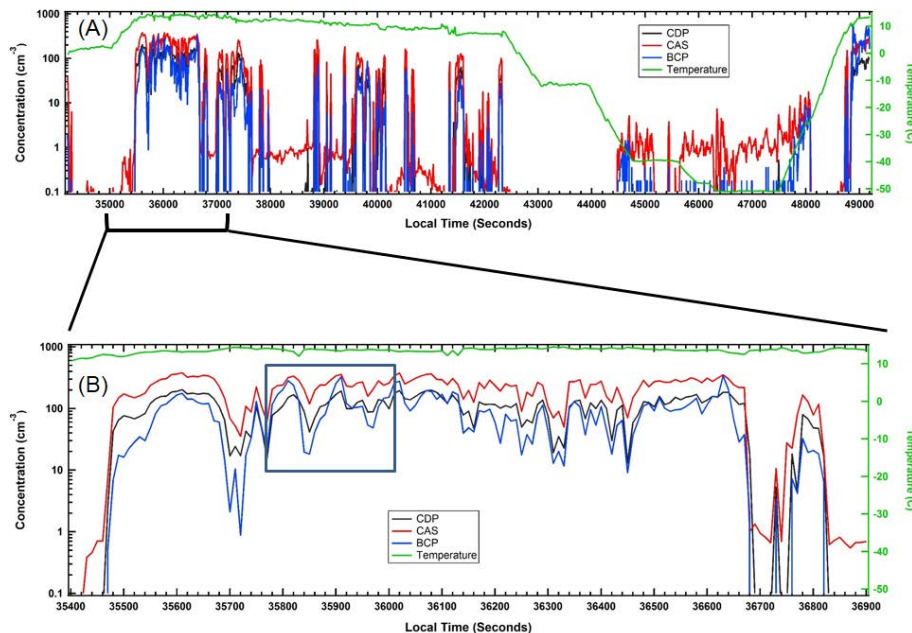
Fig. 10. In this time series of cloud particle concentrations, the CDP (black), CAS (red) and BCP (blue) are compared over the entire flight **(a)** and over an all water segment of the cloud **(b)**.
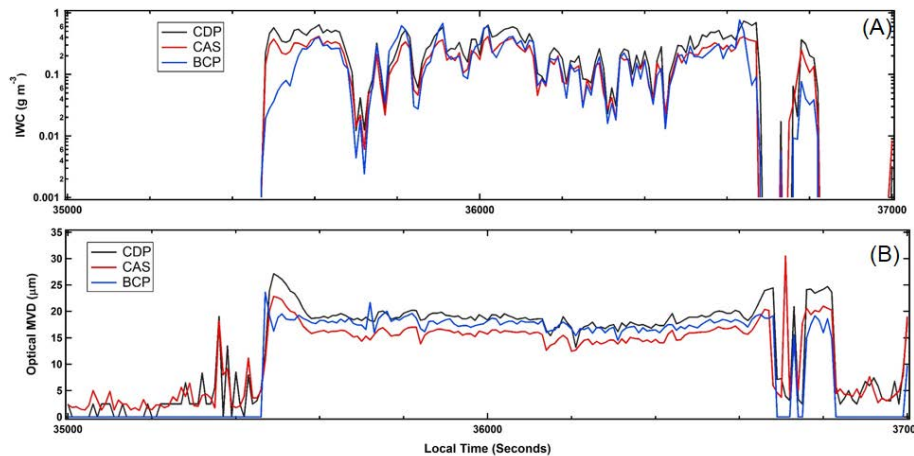
Fig. 11. These time series of liquid water content **(a)** and median volume diameter **(b)** are over the same interval of time, and in an all water cloud, as shown in Fig. 10b.
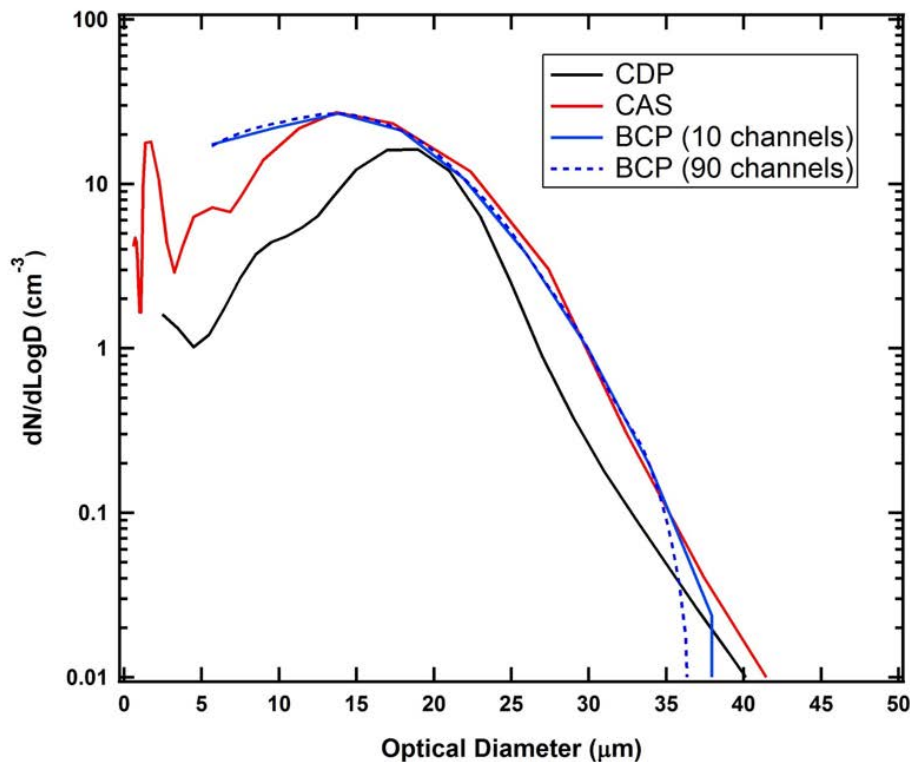
Fig. 12. The size distributions were averaged over the time period shown in Figure 10b when the aircraft was in an all water cloud. The BCP with 10 and 90 channels (blue solid and dashed) is compared to the CDP (black) and CAS (red) both instruments that have 30 channels.

Fig. 13. The BCP is shown here mounted on the Lufthansa Veirsen A340-300 Airbus, as part of the IAGOS instrument package. Also shown are the locations of the aircraft airspeed and temperature sensors.
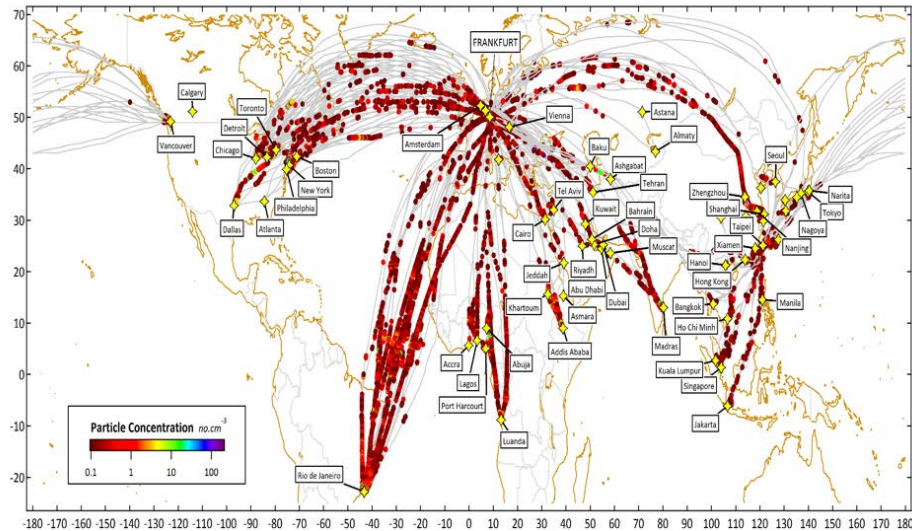
Fig. 14. The trajectories for the Lufthansa (September 2011–March 2013) and Air China (January–March 2013) commercial flights are shown here encoded with cloud encounters (colored, filled circles) and locations of arrivals and departures (yellow diamonds). The color scale shows the number concentrations of the clouds that were identified.
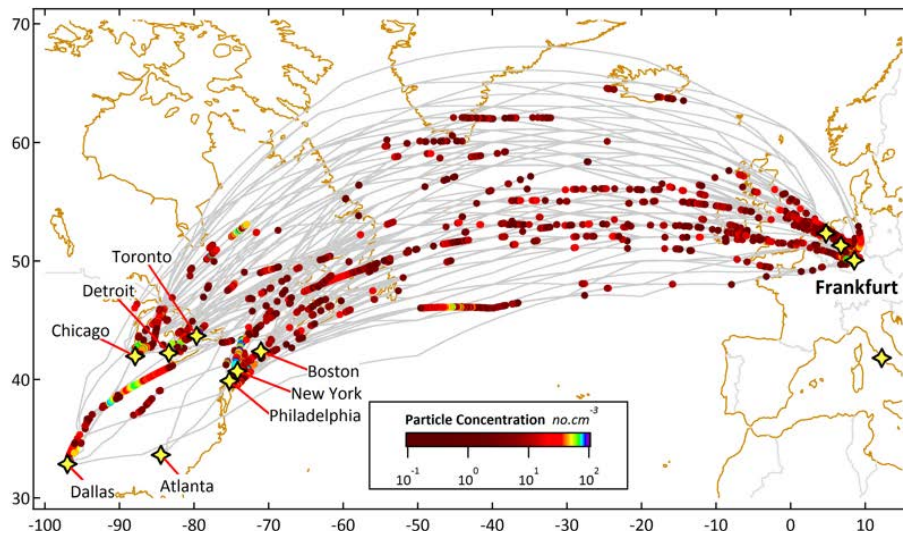
Fig. 15. Similar to Fig. 14, but expanded to show only the flights between Europe and North America.

Printer-friendly Version

Interactive Discussion
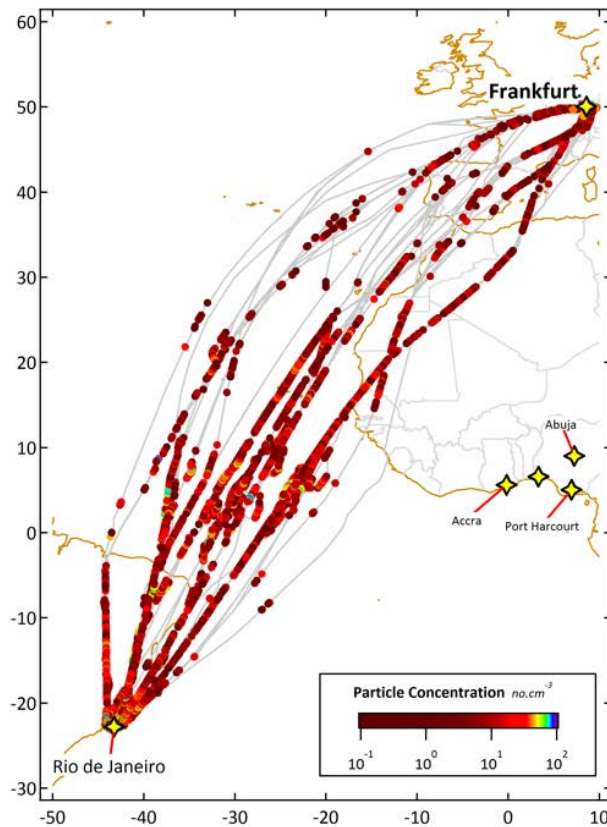
Fig. 16. Similar to Fig. 14, but expanded to show only the flights between Europe and Rio de Janeiro.

Full Screen / Esc
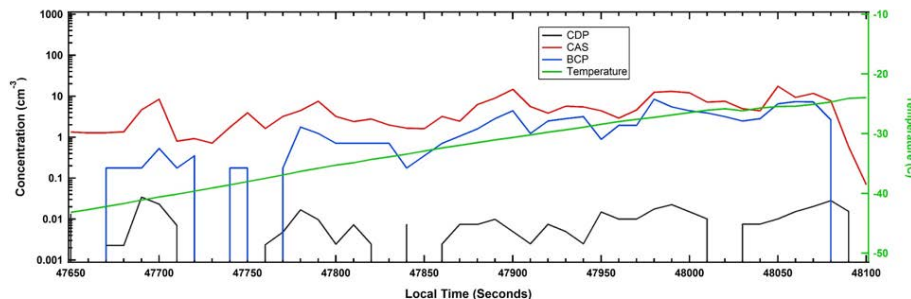
Printer-friendly Version

Interactive Discussion

Fig. 17. The CDP (black), CAS (red) and BCP (blue) number concentrations shown here illustrate the possible influence of ice crystal shattering on the measurements by the CAS and BCP in clouds where the temperature (green) indicates that the particles are probably mostly ice crystals. The CDP has no inlet and the tips on its extended arms are designed to direct shattered crystals away from the sample volume. The CAS has an inlet on which crystals shatter and the BCP could be measuring ice shards from ice crystals impacting on the fuselage upstream.
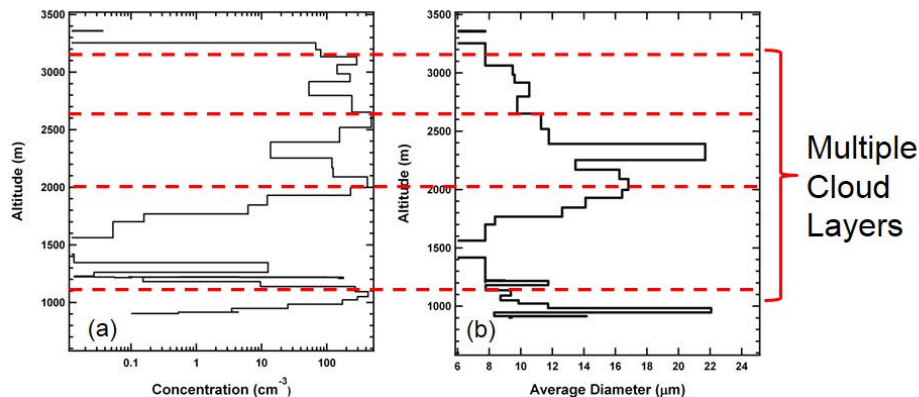
Fig. 18. These vertical profiles of the number concentration **(a)** and average optical diameter **(b)** are an example of multilayered clouds (red horizontal lines) measured with the BCP as the aircraft was landing in Frankfurt, Germany.